Bioactive Materials 16 (2022) 359–371

Contents lists available at ScienceDirect

Bioactive Materials

journal homepage: www.keaipublishing.com/en/journals/bioactive-materials

Polarization of tumor-associated macrophages by TLR7/8 conjugated radiosensitive peptide hydrogel for overcoming tumor radioresistance

Yumin Zhang [a,1], Zujian Feng [b,1], Jinjian Liu [a], Hui Li [a], Qi Su [b], Jiamin Zhang [a], Pingsheng Huang [b], Weiwei Wang [b,**], Jianfeng Liu [a,*]

[a] Key Laboratory of Radiopharmacokinetics for Innovative Drugs, Chinese Academy of Medical Sciences, and Institute of Radiation Medicine, Chinese Academy of Medical Sciences & Peking Union Medical College, Tianjin, 300192, PR China

[b] Tianjin Key Laboratory of Biomaterial Research, Institute of Biomedical Engineering, Chinese Academy of Medical Science and Peking Union Medical College, Tianjin, 300192, PR China

ARTICLE INFO

Keywords:
Radioresistance
Tumor-associated macrophage
Polarization
Immunosuppressive tumor microenvironment
Peptide hydrogel

ABSTRACT

Radioresistance reduces the antitumor efficiency of radiotherapy and further restricts its clinical application, which is mainly caused by the aggravation of immunosuppressive tumor microenvironment (ITM). Especially tumor-associated macrophages (TAMs) usually display the tumor-promoting M2 phenotype during high-dose fractional radiotherapy mediating radiotherapy resistance. Herein, the toll like receptor agonist TLR7/8a was conjugated with radiosensitive peptide hydrogel (Smac-TLR7/8 hydrogel) to regulate TAMs repolarization from M2 type into M1 type, thus modulating the ITM and overcoming the radioresistance. The Smac-TLR7/8 hydrogel was fabricated through self-assembly with nanofibrous morphology, porous structure and excellent biocompatibility. Upon γ-ray radiation, Smac-TLR7/8 hydrogel effectively polarized the macrophages into M1 type. Notably, combined with radiotherapy, TAMs repolarization regulated by Smac-TLR7/8 hydrogel could increase tumor necrosis factor secretion, activate antitumor immune response and effectively inhibit tumor growth. Moreover, TAMs repolarization rebuilt the ITM and elicited the immunogenic phenotypes in solid tumors, thus enhanced the PD1-blockade efficacy through increasing tumor infiltrating lymphocytes (TILs) and decreasing Treg cells in two different immune activity tumor mice models. Overall, this study substantiated that recruiting and repolarization of TAMs were critical in eliciting antitumor immune response and overcoming radioresistance, thus improving the efficacy of radiotherapy and immunotherapy.

1. Introduction

Radiotherapy (RT) is widely applied for solid tumor treatment in clinics, since the merits of powerful restraint on tumor growth [1,2]. It depletes cancer cells through high energy ionic radiation, inducing the double-strand breaks of DNA and eventually promoting apoptosis of cancer cells [3,4]. However, radioresistance remains the biggest obstacle hindering the curing efficacy of radiotherapy [5,6]. Causing radioresistance is multifactorial but inseparable with the special tumor microenvironment (TME) [7]. Rapid proliferation along with hypoxia are hallmarks of TME, which result in a long-term chronic inflammation circumstance around tumors and gradually facilitate the formation of immunosuppressive tumor microenvironment (ITM) [8–10]. The ITM is mainly composed by suppressive immune cells including tumor-associated macrophages (TAMs), myeloid-derived suppressor cells (MDSCs) and regulatory T cells (Treg cells), as well as certain inflammatory chemokines or cytokines like IL-10 and TGF-β [11,12]. Actually, interactions between radiation and the tumor immune system are complex that is neither wholly positive nor negative influences [13]. After radiation, secretion of inflammatory cytokines will be initiated and immune cells are recruited thus activating the immune response to attack tumors, but radioresistant immunosuppressive cells and other growth promotion factors inside TME also increased, which maintains a delicate balance between the stimulation or suppression of immune

Peer review under responsibility of KeAi Communications Co., Ltd.
* Corresponding author.
** Corresponding author.
E-mail addresses: wwwangtj@163.com (W. Wang), liujianfeng@irm-cams.ac.cn (J. Liu).
[1] These authors contributed equally to this work.

https://doi.org/10.1016/j.bioactmat.2021.12.033
Received 18 September 2021; Received in revised form 29 November 2021; Accepted 27 December 2021
Available online 3 January 2022

system [14]. Therefore, attempts to rebuild ITM is of vital significance to improve the RT efficacy and overcome radioresistance.

As natural immune cells and antigen presenting cells, macrophages play an important role in cancer development and metastasis, which could be typically divided into proinflammatory M1 macrophages and anti-inflammatory M2 macrophages [15,16]. Particularly, over 50% of immune cells in the TME are constituted by tumor-associated macrophages (TAMs). During the process of tumor progression, macrophages suffered a transformation toward M2 phenotype which would promote invasion, metastasis and angiogenesis of tumors. In addition, M2 phenotype TAMs function in many ways to weaken antitumoral immunity, including assisting the production of regulatory T cells which further worsened the ITM [17,18]. More importantly, an even worse fact is that macrophages, especially M2 type TAMs, are one of the most radioresistant cells [14,19]. A huge of anti-oxidative molecules were produced by TAMs during radiotherapy, such as manganese superoxide dismutase (MnSOD), a scavenger of superoxide (O_{-2}) ions, which confer cellular resistance against damaging effects of radiotherapy. Unfortunately, previous reports showed that an increased number of M2 type TAMs was observed after a high dose of radiation (>10 Gy), which exacerbated the ITM and led to radiotherapy failure [14,20]. Therefore, rebuilding the ITM through engineering macrophages through inhibition of M2 macrophages and repolarization of TAMs into M1 macrophages may be a feasible approach to overcome the immunosuppression and the tumor regrowth after radiotherapy.

Herein, a novel TLR 7/8 conjugated radiosensitive peptide hydrogel was fabricated to rebuild the ITM and overcome radioresistance through reprogramming macrophages polarization. In order to surmount the programming toward M2-like macrophages of TAMs resulting from high dose of irradiation, Smac mimetic peptide was chosen to improve the radiosensitivity of tumors and reduce the dose of irradiation [21,22]. During the radiotherapy, the high expression of inhibitor of apoptosis proteins (IAPs) in tumor cells can inhibit cell apoptosis and reduce the radiation sensitivity of tumors. Smac peptide can directly bind to IAPs to relieve its apoptosis-inhibiting function, thereby improving tumor radiation sensitivity [23]. Additionally, an agonist of the toll-like receptors TLR7/8 was conjugated to drive polarization of macrophages toward M1 phenotype for rebuilding the ITM [24,25]. The obtained Smac-TLR7/8 peptide could self-assemble into nanofibrous structures and forming injectable and highly porous hydrogels for local administration. After treated with the Smac-TLR7/8 peptide hydrogel accompanied with a moderate dose of γ-ray radiation, TAMs could be repolarized into an antitumor state (M1) by activating NF-κB pathways [26,27], thereby enhancing the radiotherapy efficacy. More importantly, macrophage repolarization further evoked the immune response, facilitated the recruitment of TILs and reduced the Treg cells, which contributed to relieving radioresistant TME [28,29]. In summary, such a novel strategy brings a new dawn to successfully improve the radiotherapy and overcome radioresistance by rebuilding ITM through repolarizing TAMs, activating antitumor immunity and downregulating Treg cells (Scheme 1).

2. Materials and methods

2.1. Materials

The Smac N7 peptide (Ala-Val-Pro-Ile-Ala-Gln-Lys) and the self-assembling peptide KEF9 (Lys-Lys-Phe-Lys-Phe-Glu-Phe-Glu-Phe) were

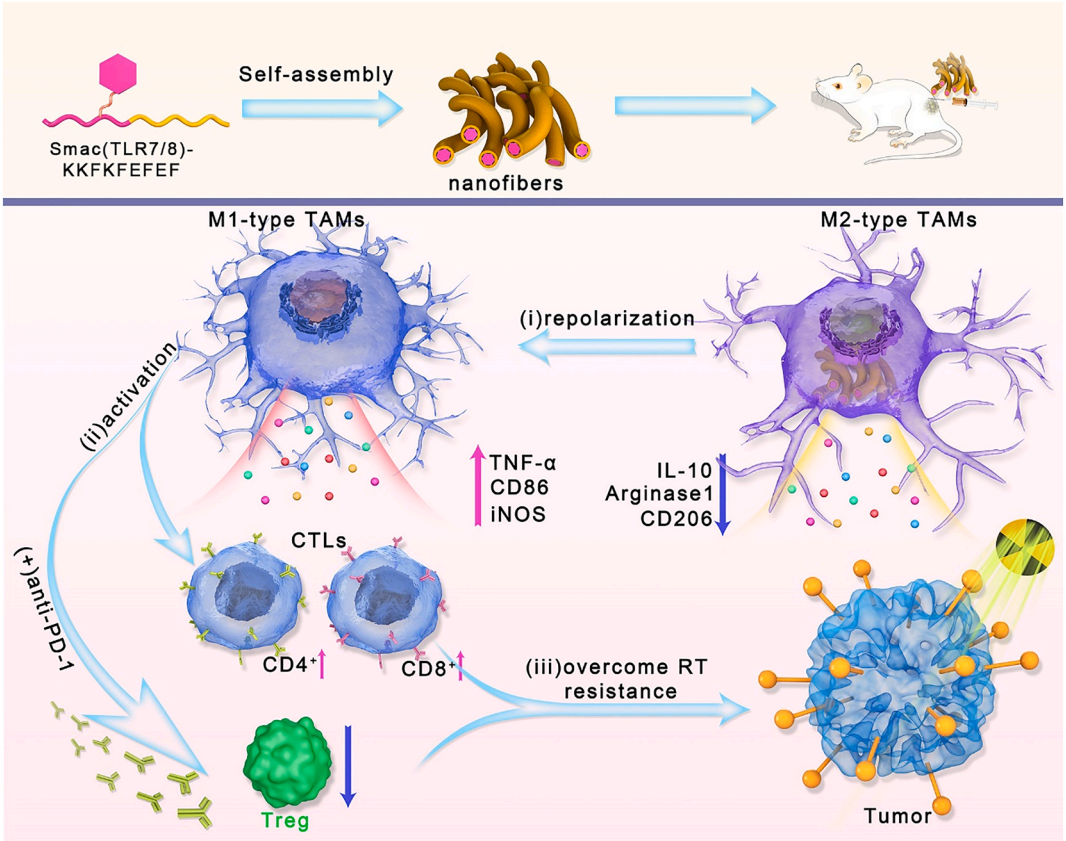

Scheme 1. Schematic illustration of the macrophage repolarization regulated by Smac-TLR7/8 hydrogel for overcoming radioresistance. The Smac-TLR7/8 peptide could self-assemble into nanofibrous hydrogel. Then, (i) After peritumoral injection, Smac-TLR7/8 hydrogel effectively reprogrammed the TAMs from M2 type toward M1 type, secreting inflammatory factors and activating anti-tumor functions. (ii) Immunosuppressive tumor microenvironment was rebuilt through tumor infiltrating lymphocytes (TILs) recruitment, and downregulating Treg cells. (iii) Thereby, the radioresistance was overcame which further improve the anti-tumor efficacy combined with immunotherapy.

obtained from Bankpeptide biological technology CO., LTD (China). Lipopolysaccharide (LPS), IL-4 and recombinant mouse monocyte colony-stimulating factor (M-CSF) were purchased from Pepro Tech (Rocky Hill, NJ, USA). Fluorochrome-labeled monoclonal antibodies (CD86, CD206, F4/80, CD3, CD4, CD8) were received from Abcam (Cambridge, UK). Primary antibodies to γ-H2AX, NF-κB, TNF-α, iNOS, IL-10, Arginase 1 and β-actin, and secondary antibodies were also purchased form Abcam (Cambridge, UK). Mouse regulatory T cell staining kit was purchased from Invitrogen (USA).

2.2. Synthesize of Smac-TLR7/8 peptide

TLR7/8a was conjugated with Smac N7 peptide through succinic acid as a linker (Smac (TLR7/8a)). And then, Smac (TLR7/8a) was coupled with KEF9 using a amidation reaction to obtain the final product Smac (TLR7/8a)-KEF9 (termed as Smac-TLR7/8).

2.3. Preparation and characterization of Smac-TLR7/8 hydrogel

Smac-TLR7/8 peptide (20 mg) was dissolved in deionized water (1.0 mL), and then the peptide hydrogel (Smac-TLR7/8 hydrogel) was assembled by dropping 10 μL of sodium chloride solution. The morphology of Smac-TLR7/8 hydrogel was analyzed by transmission electron microscopy (TEM, Hitachi H-600), and its interior morphology was evaluated by scanning electron microscope (SEM, S-4800, Hitachi, Japan) after a quick frozen and lyophilization.

The secondary structure of peptide was studied using circular dichroism (CD) spectrometer (Jasco J-810). For CD spectroscopy, Smac-TLR7/8 (100 μg) was dissolved into deionized water, the Smac-TLR7/8 solution was then incubated 2 h before scanning. The ellipticity change of Smac-TLR7/8 was scanned between 190 nm and 260 nm with an average of three scans.

The modulus of Smac-TLR7/8 hydrogel including elasticity modulus (G′) and viscosity modulus (G″) was measured by the AR2000ex rheometer. The measurements of G′ and G″ were examined over an angular frequency sweep between 1 and 10 Hz at a strain of 2.0% at 25 °C.

2.4. Biocompatibility of Smac-TLR7/8 hydrogel in vitro

Cytotoxicity test. The mouse peritoneal macrophage cell line RAW 264.7 and mouse fibroblasts cell line 3T3 cells were cultured in RPIM-1640 medium supplemented with 10% FBS (Gibco, USA), respectively. RAW264.7 was seeded in a 96-well plate with 1000 cells per well and cultured overnight. Cells were then incubated with Smac-TLR7/8 hydrogel at virous concentrations (200, 100, 50, 20, 10, 0 μg/mL). After further incubation for 24 h, CCK-8 kit was added and incubated for 1 h at 37 °C in the dark. Finally, the absorbance at 450 nm wavelength was measured using a microplate reader (Thermo Scientific, Varioskan Flash). The cytotoxicity of Smac-TLR7/8 hydrogel against 3T3 cells was also evaluated as described above.

Hemolysis Assay. Red blood cells were isolated by centrifuging at 3000 rpm and resuspended in saline solution to a final concentration of 5% (v/v). Then the Smac-TLR7/8 hydrogel with different concentrations (0.5 mL) were incubated with red blood cells suspension (0.5 mL). Triton X100 and PBS were employed as the positive and negative control, respectively. After incubation for 2 h at 37 °C, the samples were centrifuged at 3000 rpm for 5 min. Finally, the photographs of the samples were captured by a digital camera. And the supernatant was then added into a 96-well plate for measurement of the optical absorbance at 570 nm by a microplate reader. The hemolysis percentage was calculated according to the previous work.

2.5. Cell polarization experiment

Isolation of bone marrow-derived macrophages (BMDMs). Briefly, BMDMs were isolated from 5 to 6 weeks old C57BL/6 mice. After being severed, separate the femur and tibia, soak it in 75% alcohol, the muscle and connective tissue were removed from the bone, and then the tissue were rinsed with penicillin-streptomycin-containing PBS and RPIM-1640 medium. The bone marrow was flushed out using RPIM-1640 medium. After 2 min standing with 2 mL of red blood cell lysate, the cells were then diluted with 10 mL of RPIM-1640 and filtered with a 100 μm filter. After centrifugation, the cells were resuspended with RPIM-1640 medium supplemented with 10% heat-inactivated FBS and 20 ng/ml GM-CSF at 37 °C 5% CO_2 in a cell incubator for 7 days

For cell polarization studies, BMDMs cells were seeded in 6-well plates and treated with PBS, 20 nM Smac hydrogel and Smac-TLR7/8 hydrogel with or without RT (4 Gy), free TLR7/8 (20 nM) and PBS were used as controls. After further incubation for 24 h, the cells were collected and labeled with FITC-labeled anti-CD86 antibodies, PE-labeled F4/80 antibodies and APC-labeled CD206 antibodies for flow cytometry (C6, BD, USA). Polarization effect on Raw 264.7 cells was also studied as described above.

Western blot (WB) analysis. Treated BMDMs cells as described for WB analysis of NF-κB, TNF-α, iNOS, IL-10, and Arginase 1 protein expression. RIPA lysis buffer was added to each well and incubated on ice for 15 min, the samples were collected quantified with BCA protein assay kit. After SDS-PAGE electrophoresis, proteins were then transferred to PVDF membrane (0.22 μm, Millipore, USA). After blocking with the 5% skimmed milk powder for 1 h, the antibody dilution solution was used to incubate overnight at 4 °C. After washing with PBS, the HRP-labeled secondary antibody was then incubated for 2 h at room temperature. After washing with PBS, the proteins were photographed by ECL luminescence.

qRT-PCR. RNA samples of treated BMDMs cells were extracted by Trizol kit for qRT-PCR to evaluate the transcription levels of NF-κB, TNF-α, iNOS, IL-6 and IL-12 RNA. Mix the random primers and the extracted RNA, and add reverse transcriptase, 5x m-mlv reaction buffer dNTP, RNAse and water for denaturation at 70 °C for 5 min. After incubating at 37 °C for 1 h, the reaction was terminated at 70 °C for 10 min. Add each component according to the reaction system of the qRT-PCR kit, and set the qRT-PCR program. The primer sequence of each gene is as follows:

Primer	Sequence (5′to3′)
18S–F	AGAAACGGCTACCACATCCA
18S-R	TACAGGGCCTCGAAAGAGTC
TNF-α-F	CTCATGCACCACCATCAAGG
TNF-α-R	ACCTGACCACTCTCCCTTTG
NF-κB-F	ACTTCCAAGCTGAGAGGCAT
NF-κB-R	GCTGCTCCTGCAAATACTCC
iNOS-F	GTTTGCAGGCGTCAGTGTAA
iNOS-R	TCCTGAAGGAGCTTTGTCCA
IL 6-F	GACTGATGCTGGTGACAACC
IL 6-R	AGACAGGTCTGTTGGGAGTG
IL 12-F	GTGGGAGGCAACATGACATC
IL 12-R	CAGTGTGTGTGGTTCCTGTG

2.6. Repolarization experiment

BMDMs cells were seeded in 6-well plates and confocal dishes. After cultured with IL-4 (40 ng/mL) for 2 days, BMDMs cells were treated with PBS, 40 μg/mL LPS, 20 nM Smac-TLR7/8 hydrogel with 4 Gy RT. After further incubation for 24 h, the protein samples were collected for WB detection of NF-κB, TNF-α, iNOS, IL-10, and Arginase protein expression. Cells were collected and labeled with FITC-labeled anti-CD86 antibodies, PE-labeled F4/80 antibodies and APC-labeled CD206 antibodies for flow cytometric. Actin-Tracker Green-488 and CD86 antibody were used to label cells for confocal photography (C2, Nikon, Japan).

2.7. Functionalized characterization of M1-type macrophages

ELISA The BMDMs cells were seeded in a 12-well plate and treated with PBS, 20 nM free TLR7/8, 20 nM Smac-TLR7/8 hydrogel+4 Gy, respectively. After incubation for 48 h, the supernatant was collected and ELISA kit was applied to detect the concentrations of TNF-α, IFN-γ, and IL-10 according to the standard protocols. The absorbance at 450 nm wavelength was measured by the microplate reader. The concentrations (TNF-α, IFN-γ, and IL-10) of cell samples were calculated according to the protocols of Elisa kit.

Co-culture system. The transwell coculture cell system was employed to study the viability of cancer cells co-cultured with BMDMs. BMDMs cells were seeded in a 12-well plate and treated with PBS, 20 nM free TLR7/8, 20 nM Smac-TLR7/8 hydrogel+RT, respectively. After pre-incubation for 24 h, B16 cells were seeded in the 12-well plate of the transwell, and further incubated for 48 h. Then, CCK-8 kit was then added and incubated for 1 h at 37 °C in the dark, the absorbance at 450 nm wavelength was measured by the microplate reader.

2.8. Macrophage phagocytosis assay

BMDMs were seeded in 6-well plate, and incubated with 20 nM free TLR7/8, 20 nM Smac-TLR7/8 hydrogel+4 Gy, respectively. After incubation for 24 h, cells were collected and stained with the viable cell dye CMTPX (red). B16 cells were seeded in a confocal dish with 5×10^5 cells per dish and culture overnight, and then labeled with the viable cell dye CMFDA (green). The treated BMDMs cells were added to B16 at a density of $5*10^5$ cells per dish. After further incubation for 2 h, samples were washed with cold PBS and photographed using a confocal microscope. The Pearson's value, the intensity distribution relationship between the two channels of the fluorescence images, was analyzed by the ImageJ software.

2.9. γ-H2AX detect

BMDMs cells were seeded in a 12-well plate (in the lower chamber of the transwell) with 10^4 cells per well. Then cells were treated with PBS, RT (4 Gy), 20 nM Smac hydrogel, 20 nM Smac-TLR7/8 hydrogel, respectively. After incubation for 24 h, B16 cells were seeded in the upper chamber of the transwell and further incubated for 48 h. After 4 Gy radiation, B16 cells were washed with pre-cooled PBS, fixed with 4% PFA. Then the cells were permeabilized the membrane with 0.25% Triton X-100, and blocked with 3% BSA for 1 h. After that, the cells were further incubated with γ-H2AX antibody overnight at 4 °C. After washing with PBS, cells were incubated with the secondary antibody at room temperature for 2 h. Cells were stained by DAPI after being washed with PBS. The γ-H2AX within cells were finally recorded by confocal microscope.

2.10. Smac-TLR7/8 hydrogel degradation in vivo

Animals. Both BALB/c nude mice and C57BL/6 mice (18–20 g, 6–8 weeks) are purchased from Vital River Laboratory Animal Technology Co., Ltd (Beijing, China). The animal experiments including of hydrogel degradation and antitumor studies were carried out in accordance with the protocol approved by Chinese Academy of Medical Science and Peking Union Medical College and following the Guiding Principles under the Care and the Regulations for the Administration of Affairs Concerning Experimental Animals (Tianjin, revised in June 2004).

Before the in vivo antitumor studies, the degradation of Smac-TLR7/8 hydrogel was studied using in vivo imaging system (Caliper IVIS Lumina II). The Smac-TLR7/8 hydrogel was labeled with Cy5.5 through amidation reaction. After subcutaneous injection in the back of BALB/c nude mice, the fluorescence intensity was recorded and imaged by in vivo imaging system at scheduled time point. The excitation wavelength and emission wavelength were set at 675 nm and 693 nm, respectively. And the hematological analysis at various days after injection was measured by automatic blood analyzer (Celltace, Japan) to assess the in vivo biocompatibility of Smac-TLR7/8 hydrogel. Smac-TLR7/8 hydrogel labeled with Cy5.5 was peritumorally injected to identify the pharmacokinetics in the B16 tumor bearing mice. The main tissues including tumor, heart, liver, spleen, lung, and kidney were excised and imaged by an imaging system after subcutaneously peritumoral injection at schedule time points.

2.11. Antitumor effect of Smac-TLR7/8 hydrogel combining with RT in vivo

B16 cells (5×10^6) in 0.1 mL of PBS were injected into the right rear flank of C57BL/6 mice. When the tumor size arrived to ~50 mm^3, the mice were randomly divided into 6 groups (n = 10) as follows: PBS, RT, TLR7/8, Smac hydrogel+RT, Smac-TLR7/8 hydrogel and Smac-TLR7/8 hydrogel+RT. Hydrogel formulations and free TLR7/8 were peritumoral injected at an equivalent dose of TLR7/8 (2.0 mg/kg). And after injection at day 1st, 3rd and 5th, mice were radiated using ^{137}Cs gamma radiation of 3600 Ci at a radiation dose of 2.7 Gy, respectively. The tumor volume (length × $width^2$ × 0.5) and body weight were recorded every other day during the treatment. The tumor inhibition rate (TIR) was calculated using TIR (%) = $[(V_b - V_x)/V_b] \times 100$, where V_x and V_b were the tumor volumes in the treatment and blank control groups, respectively.

Cytokine detection. After the treatment, blood samples were collected and centrifuged at 5000 rpm for 8 min. The serum was obtained and used to measure the TNF-α and VEGF using ELISA kit, correspondingly.

Histopathological examination. After the mouse was sacrificed, Separate tumor tissues and organs (heart, liver, spleen, lung and kidney) and fix them with 4% paraformaldehyde. Then, the tissues were inserted in optical cutting temperature compound (OCT), and cut into 6–8 μm using freezing microtome. All the tissues were used to pathological analysis by HE staining. Ki67 and TUNEL kit were then stained to further analyze the apoptosis and proliferation of tumor cells.

To study the TAMs repolarization in the antitumor studies, tumor tissue slides were firstly stained with biomarkers-related TAMs including of FITC-labeled anti-CD86 antibodies, PE-labeled F4/80 antibodies and APC-labeled CD206 antibodies, respectively. The effect of TAMs repolarization was observed by a confocal microscope. For quantitative analysis, cells suspensions of tumor tissues were prepared by homogenization. After blocking with BSA, cells were stained with FITC-labeled anti-CD86 antibodies, PE-labeled F4/80 antibodies and APC-labeled CD206 antibodies for flow cytometric.

As for cytotoxic T Lymphocytes detection, the tumor tissues were separated, 4 ml of mouse lymphocyte separation solution (Beyotime, China) was added, after homogenization and filtration, the filtered cell suspensions were collected in a 15 ml centrifuge tube. 4 ml of RPIM-1640 medium were added and centrifuged at 1000 rpm for 10 min at 4 °C, the upper lymphocyte layer liquid was transferred to a new centrifuge tube, washed and centrifuged with PBS. The collected cell samples were then labeled with FITC-labeled CD3 antibodies, PE-labeled CD4 antibodies and APC-labeled CD8 antibodies for flow cytometric.

2.12. Overcoming radioresistance using ITM reconstruction through Smac-TLR7/8 hydrogel combining with αPD-1

B16 cells (5×10^6) in 0.1 mL of PBS were injected into the right rear flank of C57BL/6 mice. When the tumor size arrived to ~50 mm^3, the mice were divided into 4 groups (n = 10) as follows: PBS, αPD-1+RT, Smac-TLR7/8 hydrogel+RT, αPD-1+Smac-TLR7/8 hydrogel+RT. Hydrogel formulations and free TLR7/8 were peritumoral injected at an equivalent dose of TLR7/8 (2.0 mg/kg). And after injection at day 1st, 3rd and 5th, mice were radiated using ^{137}Cs gamma radiation of 3600 Ci at a radiation dose of 2.7 Gy, respectively. The αPD-1 blocking antibody

(10 mg kg^{-1}) was intraperitoneally injected at day 1st, 3rd. The tumor volume (length × $width^2$ × 0.5) and body weight were recorded every other day during the treatment.

For cytotoxic T Lymphocytes detection, the tumor tissue was separated, 4 ml of mouse lymphocyte separation solution (Beyotime, China) was added, after homogenization and filtration, the filtered cell suspensions were collected in a 15 ml centrifuge tube. 4 ml of RPIM-1640 medium were added and centrifuged at 1000 rpm for 10 min at 4 °C, the upper lymphocyte layer liquid was transferred to a new centrifuge tube, washed and centrifuged with PBS. The collected cell samples were then labeled with FITC-labeled CD3 antibodies, PE-labeled CD4 antibodies and APC-labeled CD8 antibodies for flow cytometric. And Treg cells were stained with the mouse regulatory T cell staining kit (Invitrogen, 88-8118-40), and analyzed through flow cytometry. Afterwards, the expressions of cytotoxic molecules including granzyme B and perforin secreted by $CD8^+$ T cells were examined by immunofluorescence staining methods.

For TAMs repolarization studies, tumor tissues were separated and fixed with 4% paraformaldehyde. Then, the tissues were inserted in optical cutting temperature compound (OCT), and cut into 6–8 μm using freezing microtome. Tumor tissue slides were firstly stained with biomarkers-related TAMs including of FITC-labeled anti-CD86 antibodies, PE-labeled F4/80 antibodies and APC-labeled CD206 antibodies, respectively. The effect of TAMs repolarization was observed by a confocal microscope.

2.13. Statistical analysis

Using mean ± sd presents the data, and using GraphPad Prism 8.0 performs the statistical analysis. Differences between two or multiple groups are assessed by student's t-test or one-way ANOVA, denoted by $^*p < 0.05$, $^{**}p < 0.01$, and $^{***}p < 0.001$.

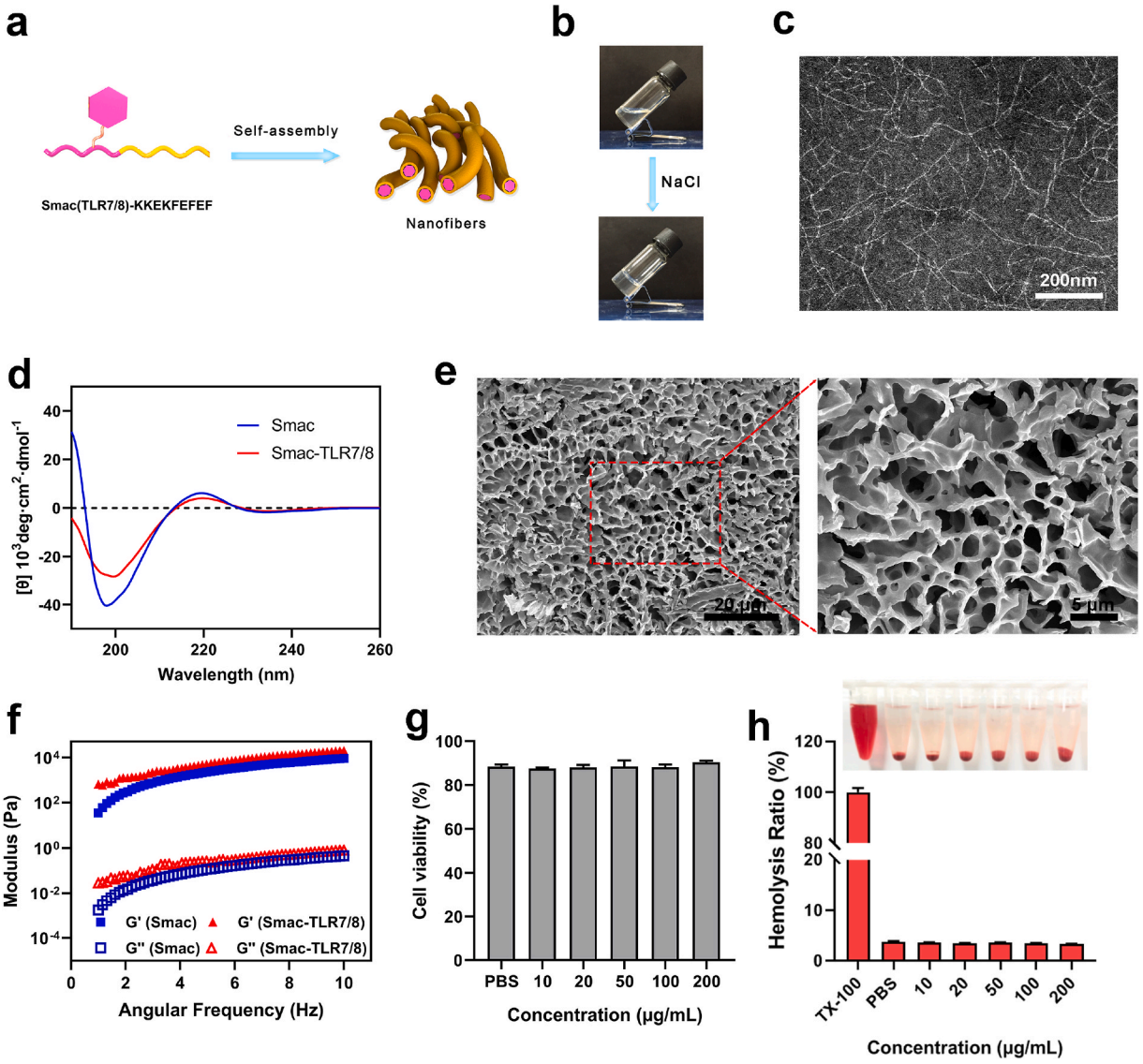

Fig. 1. Characterizations of Smac-TLR7/8 hydrogel. (a) Schematic diagram of self-assembly of Smac-TLR7/8 hydrogel. (b) Digital photograph of sol-to-gel transition of Smac-TLR7/8 hydrogel at a concentration of 20 mg/mL induced by sodium chloride. (c) TEM image of Smac-TLR7/8 nanofibers. (d) Circular dichroism (CD) spectrum of Smac-TLR7/8 hydrogel. (e) SEM image of Smac-TLR7/8 hydrogel. (f) Rheological analysis of Smac-TLR7/8 hydrogel as a function of angular frequency. (g) Cytotoxicity of 3T3 cells treated with Smac-TLR7/8 hydrogel with different concentrations. (h) Hemolysis analysis of Smac-TLR7/8 hydrogel with different concentrations.

3. Results and discussion

3.1. Synthesize and characterization of Smac-TLR7/8a hydrogel

Peptide-based hydrogel has versatile advantages including high water content, tunable mechanical properties, excellent biocompatibility and injectability, which has been widely applied in biomedical field, especially in nanomedicine and other potent techniques for cancer therapy [30,31]. According to the synthetic route of Fig. S1a, the TLR7/8a (imiquimod) conjugated peptide (Smac (TLR7/8a)-KKFKFEFEF, Smac-TLR7/8) was successfully synthesized by conjugating TLR7/8 agonist to peptide (AVPIAQK-KKFKFEFEF, Smac-KKEF), which was confirmed by liquid chromatograph-mass spectrometer (LC-MS) (Figs. S1b and c, Fig. S2) and Fourier Transform infrared spectroscopy (FTIR) (Fig. S3). As shown in Fig. 1a and b, the Smac-TLR7/8 could self-assemble into nanofibrous structures and form a transparent hydrogel with the addition of several drops of sodium chloride solution. The transmission electron microscope (TEM) image indicated that the

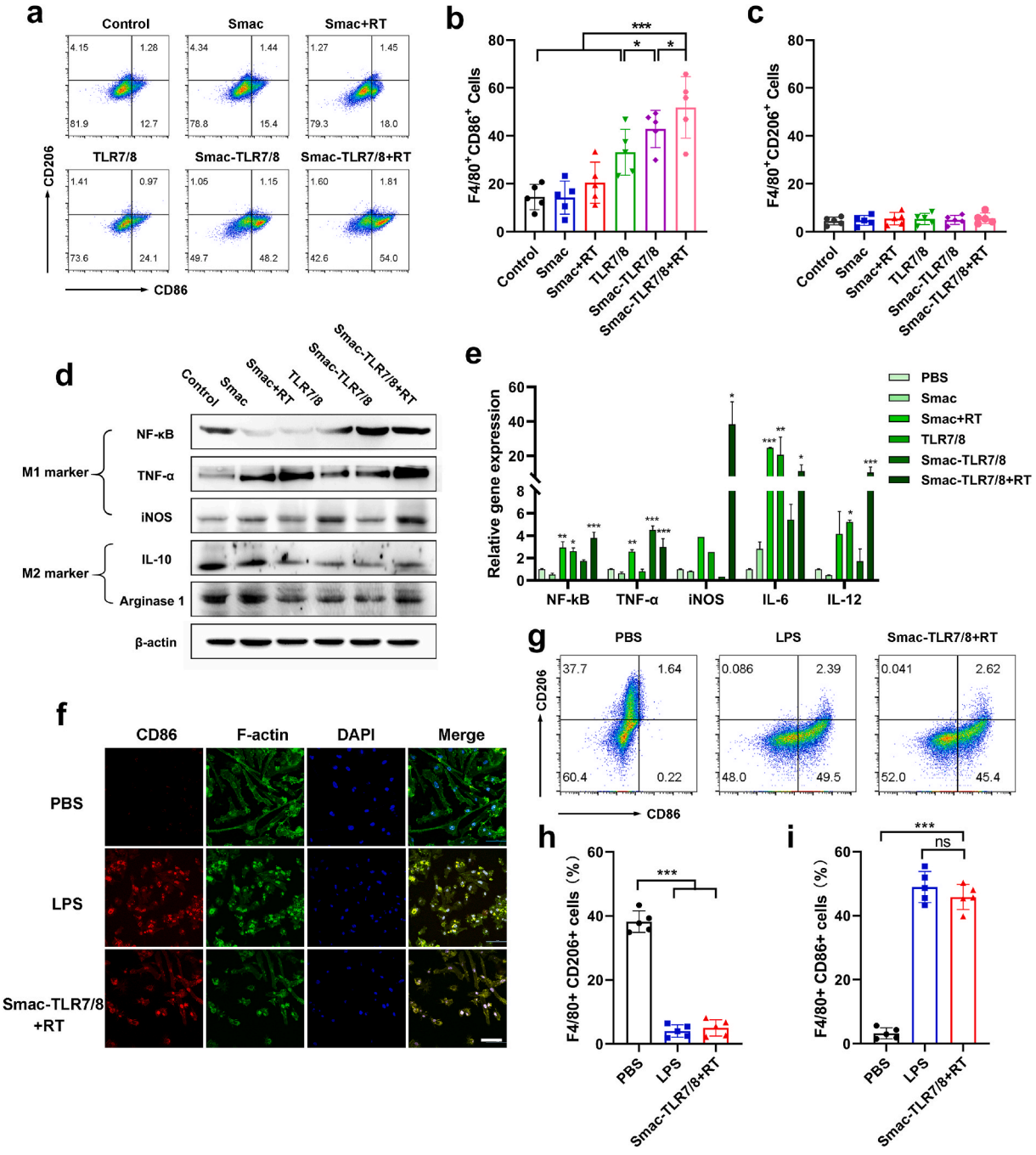

Fig. 2. Smac-TLR7/8 hydrogel re-educated macrophages toward M1 type. (a) Flow cytometry analysis of CD86 and CD206 expression (gated on F4/80$^+$ cells). (b) Percentage of M1-related (F4/80$^+$CD86$^+$) macrophages (n = 5). *p < 0.05, ***p < 0.001. (c) Percentage of M2-related (F4/80$^+$CD206$^+$) macrophages (n = 5). (d) Protein expression level of NF-κB, TNF-α, iNOS, IL-10, Arginase 1 in macrophages determined by western blotting. (e) The gene expression of NF-κB, TNF-α, iNOS, IL-6 and IL-12 mRNAs compared by qRT-PCR (n = 3). (f) Representative CLSM images of BMDMs after treated by LPS, Smac-TLR7/8 hydrogel+RT (red: CD86; green: F-actin; blue: cell nuclear). (g) Flow cytometry analysis of CD86 and CD206 expression (gated on F4/80$^+$ cells). (h) Percentage of M1-related (F4/80$^+$CD86$^+$) macrophages (n = 5). ***p < 0.001. (i) Percentage of M2-related (F4/80$^+$CD206$^+$) macrophages (n = 5). ***p < 0.001. (For interpretation of the references to colour in this figure legend, the reader is referred to the Web version of this article.)

hydrogel displayed compact nanofibrous and three-dimensional networks with the width in the range of 5–10 nm and length in the magnitude of micrometer (Fig. 1c). Circular dichroism (CD) spectroscopy was used to study the secondary structure of Smac-TLR7/8 hydrogel. As shown in Fig. 1d, Smac-TLR7/8 peptide solution displayed a negative peak at 200 nm and a positive weak band at 220 nm, which were attributed to random coil. Based on these results, the supramolecular self-assembly of Smac-TLR7/8 was possibly driven by electrostatic interactions among KKFKFEFEF, hydrogen bonding, and hydrophobic interactions among Smac peptide and TLR7/8 [32].

Next, scanning electron microscope (SEM) was utilized to evaluate the morphology of Smac-TLR7/8 hydrogel. As shown in Fig. 1e, Smac-TLR7/8 hydrogel exhibited a uniform and compact network with highly porous structure, which was beneficial as carriers for proteins/drug delivery. From the rheology analysis (Fig. 1f), the value of storage modulus G′ was much higher than that of loss modulus G″, indicating a stable gel state of Smac-TLR7/8 assembly at a peptide concentration of 20 mg/mL. In addition, the modules of Smac-TLR7/8 hydrogel were slightly higher than that of Smac hydrogel, which was mainly owing to the hydrophobic interaction of TLR7/8 reinforcing the nanofibrous structure of self-assembled peptides.

Subsequently, the biocompatibility of Smac-TLR7/8 hydrogel was studied by CCK-8 assay. As shown in Fig. 1g and Fig. S4, after incubated with Smac-TLR7/8 hydrogel for 24 h, both 3T3 cells and RAW264.7 cells showed a high cell viability. And Fig. S5 demonstrated that the Smac-TLR7/8 hydrogel could inhibit the proliferation of B16 cells and displayed a concentration-dependent manner, which was mainly attributed to the promoting apoptosis effect of Smac peptide. These results indicated a favorable biocompatibility of Smac-TLR7/8 hydrogel and a selectivity of promoting apoptosis of Smac peptide [33]. Additionally, a lower hemolysis ratio of Smac-TLR7/8 hydrogel further guaranteed its blood biocompatibility (Fig. 1h).

3.2. Polarization and repolarization of macrophages in vitro

As a toll-like receptor, TLR7/8 agonists can activate related pathways to polarize macrophages into M1 type [24]. And previous studies also showed that a moderate dose of X-ray irradiation could upregulate the pro-inflammatory M1 phenotype macrophages and downregulate the anti-inflammatory M2 phenotype macrophages [14]. Therefore, we preliminarily studied the in vitro biological activity of the Smac-TLR7/8 hydrogel under a moderate dose radiation (4 Gy) on macrophage polarization. Bone marrow derived macrophages (BMDMs) were incubated with PBS, free TLR7/8, Smac hydrogel, Smac-TLR7/8 hydrogel, respectively. Firstly, the macrophages polarization was certificated by CD86 and CD206 staining and analyzed by Flow cytometry, which were the typical biomarkers for M1 type and M2 type macrophages, respectively [34]. As shown in Fig. 2a, most BMDMs treated with PBS and Smac hydrogel were in an unpolarized state. While upon Smac hydrogel treatment with γ ray radiation, parts of primary BMDMs shifted into M1 type macrophages, verifying that a moderate dose of γ ray radiation could promote the macrophages polarization toward M1-type. Furthermore, as shown in Fig. 2b, compared to free TLR7/8 treatment (33.1 ± 9.6%), the M1 type ($F4/80^+CD86^+$) macrophages were increased (42.9 ± 7.8%) after treatment with Smac-TLR7/8 hydrogel, indicating an improved bioactivity of TLR7/8. It might be due to the fact that the conjugating in nanofibrous peptide could improve the stability and availability of TLR7/8 [35,36]. More importantly, upon γ ray radiation, proportion of M1 phenotype macrophages was significantly elevated (51.8 ± 12.8%) in Smac-TLR7/8 hydrogel group (Fig. 2b), while M2 type macrophages were not significantly affected and kept up a low level (Fig. 2c), which highlight its capability on macrophage polarization toward M1 phenotype. Similarly, Smac-TLR7/8 hydrogel combined with RT achieved the best polarization effect on macrophages toward M1 type on RAW264.7 cells (Fig. S6).

Furtherly, the level of several kinds of M1 and M2-type macrophages associated with protein expression was evaluated by western blot (WB). As shown in Fig. 2d and Fig. S7, compared with the control group, the level of M1 related proteins including NF-κB, TNF-α and iNOS were significantly upregulated in BMDMs after treated with Smac-TLR7/8 hydrogel with RT, while downregulating the level of M2 related protein expression (IL-10, Arginase 1). Real-time PCR analysis was employed to further identify the inflammation response of macrophages. Previous have shown that TLR7/8 agonists promoted macrophage polarization through activating NF-κB pathway and inducing the secretion of proinflammatory cytokines [27,37]. As shown in Fig. 2e, Smac-TLR7/8 hydrogel with RT upregulated the level of gene expression of NF-κB, confirming the inherent polarization effect of Smac-TLR7/8 hydrogel combining with RT mediating through NF-κB pathway. Moreover, the proinflammatory cytokines including TNF-α, iNOS, IL-6 and IL-12 were all upregulated, suggesting the proinflammatory response after treatment of Smac-TLR7/8 hydrogel combined with RT.

It was known that macrophages are one of the highly dynamic and plastic cells within the tumor microenvironment [38]. Dysregulation of macrophages phenotype and returning to the tissue specific baselines are increasingly recognized to have an important role in the fate of the ITM [39,40]. Therefore, rebuilding ITM by repolarizing macrophage from M2 type into M1 type is of importance in overcoming radioresistance. We next study the TAMs repolarization stimulated by Smac-TLR7/8 hydrogel during RT. And lipopolysaccharide (LPS) was used as the positive control. BMDMs was pre-incubated with IL-4 to enable it to manifest M2 phenotype macrophages, then further incubated with PBS, LPS or Smac-TLR7/8 hydrogel with RT. As shown in Fig. 2f, for PBS group, cell morphology displayed elongated structure, which was the typical morphology of M2 type macrophages, and exhibited low expression level of M1 phenotype biomarkers (CD86). After treated with Smac-TLR7/8 hydrogel with RT, cell morphology obviously shifted to pseudopod-like structures and the CD86 biomarker was overexpressed, which was consistent with the result of LPS treatment (Fig. 2f). Furthermore, macrophage repolarization was quantificationally studied using flow cytometry. As shown in Fig. 2g–i, cells treated with PBS displayed higher M2 macrophage population ($F4/80^+CD206^+$) than that of Smac-TLR7/8 hydrogel+RT. While Smac-TLR7/8 hydrogel+RT treatment significantly elevated the M1 macrophage population ($F4/80^+CD86^+$), which had no difference with LPS group. Western blot results also revealed that M2 macrophage related markers (IL-10, Arginase 1) were downregulated after treatment of Smac-TLR7/8 hydrogel+RT, while M1 related markers (NF-κB, TNF-α) were upregulated (Fig. S8). Therefore, these results suggested that Smac-TLR7/8 hydrogel+RT has intrinsic ability to re-educate macrophage from M2 phenotype toward M1 phenotype.

3.3. Functionalized characterization of the polarized M1 type macrophages

As vital natural immune cells, macrophages, especially M1 type macrophages, eliminate necrotic tissue and cancer cells through secreting tumor necrosis factor, direct phagocytosis of cancer cells and evoking the antitumor immune response as antigen presenting cells [34,41]. Accordingly, the biological functions of the polarized M1 type macrophages were evaluated. Firstly, the concentration of typical inflammatory cytokines secreted by macrophages was tested after treatment with Smac-TLR7/8 hydrogel with RT by enzyme-linked immunosorbent assay (ELISA). As shown in Fig. 3a, the Smac-TLR7/8+RT treatment significantly upregulated M1-associated cytokines (TNF-α, IFN-γ) and downregulated M2-associated cytokines (IL-10). Particularly, the level of TNF-α sharply increased over ~3 fold compared with the free TLR7/8 group and ~10 fold compared with blank group, respectively. The transwell coculture cell system was employed to study the inhibiting effect on tumor cells of BMDMs [29]. As illustrated in Fig. 3b, BMDMs were pre-incubated with TLR7/8 or Smac-TLR7/8+RT in the lower chamber of the transwell, and then

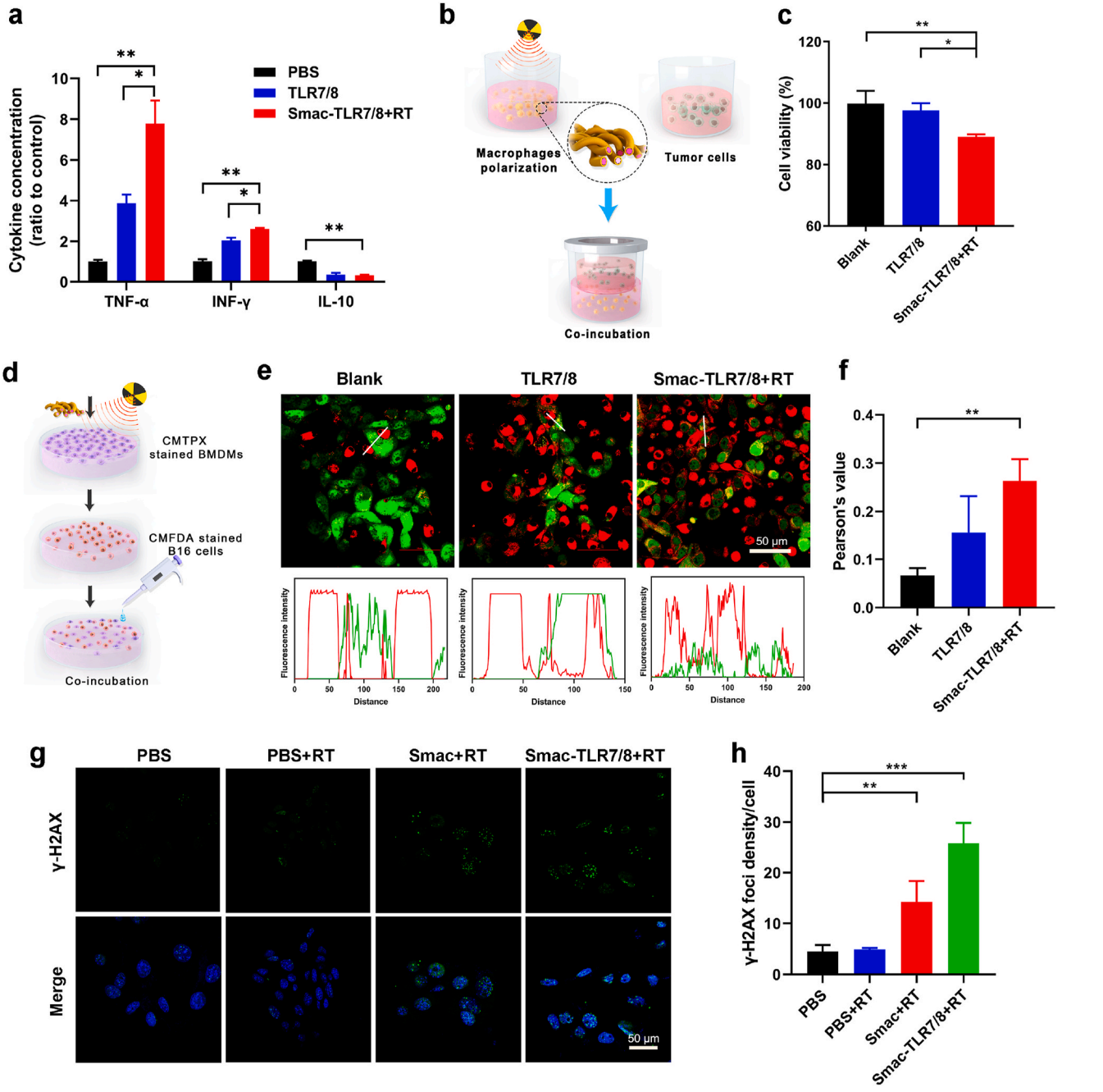

Fig. 3. Functionalized characterizations of M1 macrophages educated by Smac-TLR7/8 hydrogel+RT. (a) The level of cytokines including TNF-α, IFN-γ, IL-10 in the BMDMs cells culture supernatant detected by ELISA (n = 3). (b) The flowchart of the transwell co-culture cell system. (c) The viability of B16 cells in the upper chamber of the transwell co-culture cell system (n = 3). *p < 0.05. **p < 0.01. (d) Schematic representation of phagocytosis assay of BMDMs after treated with different formulations. (e) Representative confocal images of phagocytosis assays. Scale bar: 20 μm. B16 cells were stained with CMFDA (green), and BMDMs were stained with CMTPX (red). (f) Histogram of co-localization index between CMPTX stained BMDMs and CMFDA stained B16 cells. **p < 0.01. (g) Immunofluorescent imaging of γ-H2AX foci within B16 cells after treated with PBS, Smac hydrogel and Smac-TLR7/8 hydrogel under 6 Gy radiation. Scale bar: 50 μm. (h) Quantitative analysis of γ-H2AX foci in B16 cells after treated with PBS, Smac hydrogel and Smac-TLR7/8 hydrogel under 6 Gy radiation (n = 3). **p < 0.01, ***p < 0.001. (For interpretation of the references to colour in this figure legend, the reader is referred to the Web version of this article.)

co-cultured with B16 cells in the upper chamber for further 24 h. The results in Fig. 3c shown that the proliferation of B16 cancer cells co-cultured with BMDMs stimulated by Smac-TLR7/8+RT reduced about 14%, which was higher than that of free TLR7/8 group, benefiting from the tumor necrosis factor secreted by polarized M1 type macrophages. To study the phagocytosis ability of macrophages, BMDMs cells were incubated with free TLR7/8 and Smac-TLR7/8+RT (Fig. 3d). As shown in Fig. 3e, an obvious "don't eat me" phenomenon can be directly observed from blank group, which had no interaction between BMDMs (red) and B16 cells (green), showing a poor capacity of phagocytosis of the unpolarized macrophages [42]. Afterwards, the co-localization between CMFDA stained B16 cells (green) and CMTPX stained BMDMs (red) treated with TLR7/8 was recorded by CLSM, indicated that the cancer cells were phagocytosed by the polarized BMDMs. In particular, after treated with Smac-TLR7/8+RT, the phagocytic capacity of macrophages was further intensified (Fig. 3e), which was also confirmed by quantitatively analyzing the co-localization Pearson's value of macrophages and cancer cells (Fig. 3f). Lastly, the effect of macrophage

polarization on radiosensitivity was further evaluated (Fig. 3b). As shown in Fig. 3g, DNA double strands breakage were observed in both Smac hydrogel and Smac-TLR7/8 hydrogel with RT group. Particularly, treatment of Smac-TLR7/8+RT exhibited the most aggravated DNA breakage (Fig. 3h), emphasized that M1 macrophages could increase the radiosensitivity of cancer cells, attributing to the secretion of pro-inflammation cytokines and producing oxidative molecules including reactive oxygen species (ROS), nitric oxide (NO) and so on [43]. Overall, antitumor functions of macrophages were significantly improved after being regulated into M1 phenotype, indicating that activating M1 phenotype is much indispensable for macrophages to engage in inhibiting tumor growth.

3.4. Immunotherapy activation by TAMs repolarization stimulated by Smac-TLR7/8 hydrogel

Firstly, the in vivo degradation of Smac-TLR7/8 hydrogel was studied by in vivo fluorescence imaging through conjugating a fluorescence dye (Cy5.5). As shown in Fig. S9, after subcutaneously injected with Smac-TLR7/8 hydrogel, strong fluorescent signal of Cy5.5 was showed in the subcutaneous injection site at the beginning, and exhibited a slow degradation kinetics as time lasted. From Fig. S9b, about 50% and 75% of hydrogel were degraded after 3 days and 7 days injection. Until 14 days, all the hydrogel was degraded in vivo. Meanwhile, during the hydrogel degradation in vivo, the hematology index (WBC, LYM, RBC, HGB, MCV, PLT) after 3, 7, 14 days subcutaneous implantation ranged within a normal level compared with control group (Fig. S10), guaranteeing the in vivo biosafety of Smac-TLR7/8 hydrogel. Furtherly, the tissue distribution of Smac-TLR7/8 hydrogel was conducted to identify

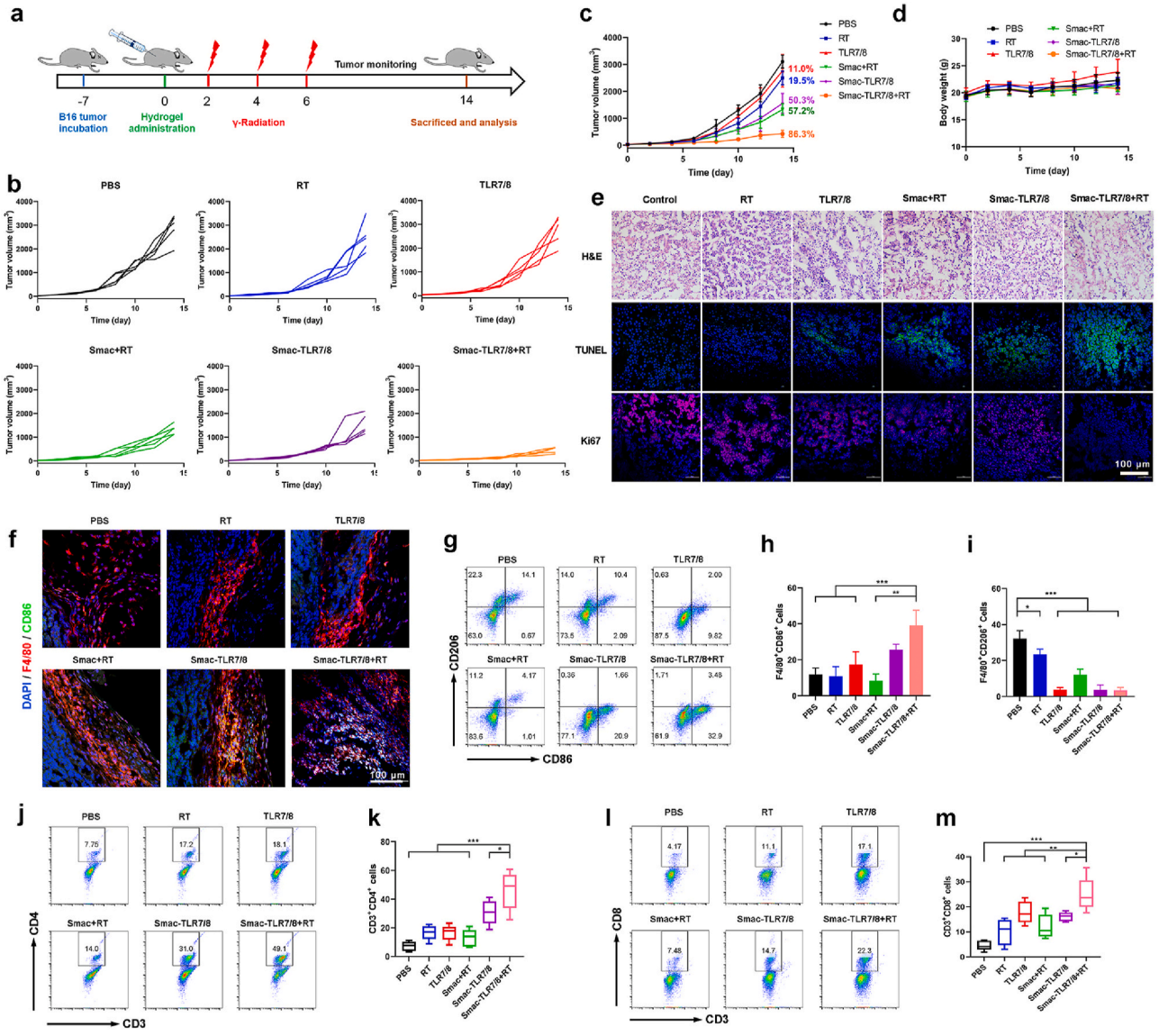

Fig. 4. In vivo tumor treatment of Smac-TLR7/8 hydrogel during radiotherapy. (a) Schedule for tumor treatment. (b) Tumor volume curve from individual mouse of different treatment groups. (c) Overall tumor volume curves and body weight (d) of different treatment groups (n = 5). The numbers represented for tumor inhibition of different treatment groups. (e) Representative images for H&E, TUNEL, and Ki67 staining of tumor tissue slides. Scale bar: 50 μm. (f) Representative images for F4/80$^+$CD86$^+$ staining of tumor tissues. Scale bar: 100 μm. (g) Flow cytometry analysis of CD86 and CD206 expression (gated on F4/80$^+$ cells). (h) Percentage of M1-related (F4/80$^+$CD86$^+$) macrophages (n = 5). **p < 0.01, ***p < 0.001. (i) Percentage of M2-related (F4/80$^+$CD206$^+$) macrophages (n = 5). *p < 0.05, ***p < 0.001. (j) Flow cytometry analysis of CD3$^+$CD4$^+$ T cells. (k) Percentage of CD3$^+$CD4$^+$ T cells (n = 5). *p < 0.05, ***p < 0.001. (l) Flow cytometry analysis of CD3$^+$CD8$^+$ T cells. (m) Percentage of CD3$^+$CD8$^+$ T cells (n = 5). *p < 0.05, **p < 0.01, ***p < 0.001.

the pharmacokinetics in the B16 tumor bearing mice. The Representative fluorescence imaging of tumors and quantification of fluorescence intensity of main organs was shown in Fig. S11. Results demonstrated that tumor tissues had the highest fluorescence intensity, indicating among of Smac-TLR7/8 hydrogel cumulated in tumor tissues after peritumoral injection. And the fluorescence intensity decreases over time owing to the degradation of the Smac-TLR7/8 hydrogel. Additionally, peritumorally administrated Smac-TLR7/8 hydrogel yielded dramatically lower accumulation in the heart, liver, spleen, lung and kidneys, avoiding the off-target effect.

Subsequently, the effect of Smac-TLR7/8 hydrogel on inhibition of tumor growth combined with radiotherapy in vivo was evaluated using B16 tumor bearing C57/BL mice. The treatment was carried out according to the procedure illustrated in Fig. 4a. Considering that the Smac-TLR7/8 hydrogel could form in situ through self-assembly, it was beneficial for peritumoral injection to avoid the side effects and enhance the therapeutic efficiency [22]. As shown in Fig. 4b and c, free TLR7/8 treatment displayed poorest tumor inhibition rate of 11% due to its low solubility and bioavailability in vivo. While conjugating with Smac peptide, the Smac-TLR7/8 hydrogel could prolong the retention time and availability of TLR7/8, further enhancing its antitumor effect (50.3% of tumor inhibition rate). Additionally, comparing with the RT treatment groups, pro-apoptotic peptides (Smac N7) commendably improved the radiosensitivity of tumors with 57.2% of tumor inhibition rate, which could avoid high dose of irradiation causing programming TAMs toward M2-like macrophages and further deterioration of radioresisitence. Most importantly, treatment with Smac-TLR7/8+RT exhibited the best tumor inhibition effect (86.3% of tumor inhibition rate) during 14 days, owing to the synergistic effect of radiotherapy and improvement of ITM through TAMs repolarization. Furthermore, tumor sections analysis including Hematoxylin/eosin (H&E) staining, TUNEL assay and Ki67 assay (Fig. 4e) also indicated that the most serious tumor necrosis, highest cell apoptosis level and poorest cell proliferation capacity were achieved after receiving treatment of Smac-TLR7/8 hydrogel combing with RT, which was in line with the tumor growth inhibition. During the whole treatment, there was no obvious change in the body weight and maintained a natural growth of mice (Fig. 4d). And no obvious damages were observed from the major organs (heart, liver, spleen, lung and kidney) through H&E staining (Fig. S12). These results indicated that such antineoplastic protocols were safe and did not cause severe side effects.

To study whether the antitumor functions are attributed to the TAMs repolarization toward M1 phenotype, macrophages populations in the tumor tissues were evaluated. As shown in Fig. 4f, immunofluorescence staining results preliminarily revealed that little $F4/80^+CD86^+$ cells distributed in tumor tissues after treated with TLR7/8, while Smac-TLR7/8 hydrogel and Smac-TLR7/8 hydrogel+RT group showed the most distribution of $F4/80^+CD86^+$ cells. After quantitative analysis using flow cytometry (Fig. 4g–i), the TAMs within the tumor tissues were mainly composed of M2 phenotype ($F4/80^+CD206^+$) in PBS and RT groups, while there was scarcely expression of M1 phenotype TAMs ($F4/80^+CD86^+$), which could contribute to the fastest growth of tumors in these two groups. Conflicted to the tumor inhibition results that Smac+RT group could exert moderate antitumor effect, as shown in Fig. 4e, higher M1 phenotype macrophages were found in the Smac+RT group, indicated that moderate dose of irradiation could elicit macrophages polarization toward M1 type. But the antitumor effect of Smac+RT was mainly attributed to pro-apoptotic effect of Smac peptide during RT rather than TAMs repolarization [33]. Notably, Smac-TLR7/8+RT group exhibited much higher population of M1 type macrophages ($F4/80^+CD86^+$) and lowest population of M2 type macrophages ($F4/80^+CD206^+$) than that of other groups (Fig. 4g and h). These results suggested that TAMs repolarization mediated by TLR7/8a enhanced the radiosensitivity of tumors and promoted the efficacy of radiotherapy combined with the pro-apoptotic effect of Smac N7 peptide, thus contributing to the superior antitumor efficacy.

It is well known that M2 type TAMs could inhibit the infiltration and antitumor functions of tumor-infiltrating lymphocytes (TILs), thus exacerbating ITM and promoting the tumor growth [44]. We furtherly evaluated the anti-cancer immune response activation by the TAMs repolarization. The quantitative analysis of cytotoxic T lymphocytes ($CD8^+$ T cells) and Th1 cells ($CD4^+$ T cells) after various treatments were shown in Fig. 4j-m. It was shown that expressions of both cytotoxic $CD8^+$ T cells and $CD4^+$ T cells were significant upregulated after treatment with Smac-TLR7/8+RT, displaying obvious differences compared with free TLR and other treatment groups. As TAMs repolarization toward M1 type has the ability to increase the secretion of pro-inflammation cytokines and inhibit the anti-inflammation, which also committed to elite antitumor immune response. As shown in Fig. S13, the level of M1 related pro-inflammation cytokines, TNF-α, in the mice serum was significantly upregulated, while the anti-inflammation cytokines of VEGF (M2 related cytokines) were downregulated after treatment with Smac-TLR7/8+RT, attributing to the reprogramming of TAMs in the tumor tissues which weaken the suppression on T cells caused by the ITM, activating $CD4^+$ and $CD8^+$ T cells and improving their infiltration into tumors.

3.5. Overcome radioresistance by downregulating treg through TAMs repolarization

Regulatory T cells (Treg cells), as an important immune cell contributing to ITM, exhibited significant upregulation during the high dose of radiotherapy, thus leading to tumor radioresistance [17,18,20]. Therefore, abrogation of Treg suppression is the main strategy of the combined radiotherapy and immunotherapy in clinical tumor therapy. Combination therapy between immune checkpoint blockade and RT led to a significant tumor growth inhibition by enhancing cytotoxic T lymphocytes and decreasing Tregs, but it is still not durable and tumor recurrent [13,18]. Since Smac-TLR7/8+RT could effectively reprogram TAMs from M2 type toward M1 type in vitro and in vivo, and regulate the expression of related inflammation cytokines. Among them, IL-10 secreted by M2 type TAMs was considered highly relevant with the accumulation of Treg cells in tumor tissues [45]. Therefore, we hypothesized that the Tregs expression can be abrogated by the strategy of TAMs repolarization, thus overcoming tumor radioresistance. Herein, we evaluated the capacity of Smac-TLR7/8+RT on abrogation of Tregs within tumor mice models with different immune activity, which the clinical combination therapeutic strategy (αPD-1+RT) was used as the control. Mice were randomly divided into four groups and received treatments of PBS, αPD-1+RT, Smac-TLR7/8+RT and Smac-TLR7/8+RT+αPD-1, respectively. As shown in Fig. 5a and b, compared with PBS treatment, the tumor growth of all mice was significantly suppressed in another three treatment groups. Apparently, the tumor inhibition rate of Smac-TLR7/8+RT (67.7%) was much higher than that of αPD-1+RT treatment (36.2%) by calculating the volume of tumors. This can be explained by that the different levels of cancer immunotherapy activation and the depletion of Tregs, evidenced by both the populations of $CD8^+$ T cells and $CD4^+$ T cells of Smac-TLR7/8+RT group was higher than that of αPD-1+RT group at 14 days treatment (Fig. 5c and d, Figs. S14 and S15). Moreover, after treatment with Smac-TLR7/8+RT, the depletion of Tregs was furtherly enhanced (9.4%, $Foxp3/CD4^+$ T cells), attributing to TAMs repolarization from M2 type to M1 type (Fig. S16). In a feedback, depletion of Tregs contributed to the higher antitumor efficiency by alleviating or overcoming tumor radioresistance. Thus, a best tumor inhibition rate (73.8%, Fig. 5a and b) was achieved after receiving the combination therapy (αPD-1+Smac-TLR7/8+RT), benefiting from the significant anti-tumor immune response and alleviating tumor radioresistance through macrophage repolarization (Fig. 5c–f, Figs. S14–S16). Whereas, there had no difference of tumor inhibition rate between Smac-TLR7/8+RT and αPD-1+Smac-TLR7/8+RT, speculated that it may be due to the higher immune activity of the B16 tumor model. In

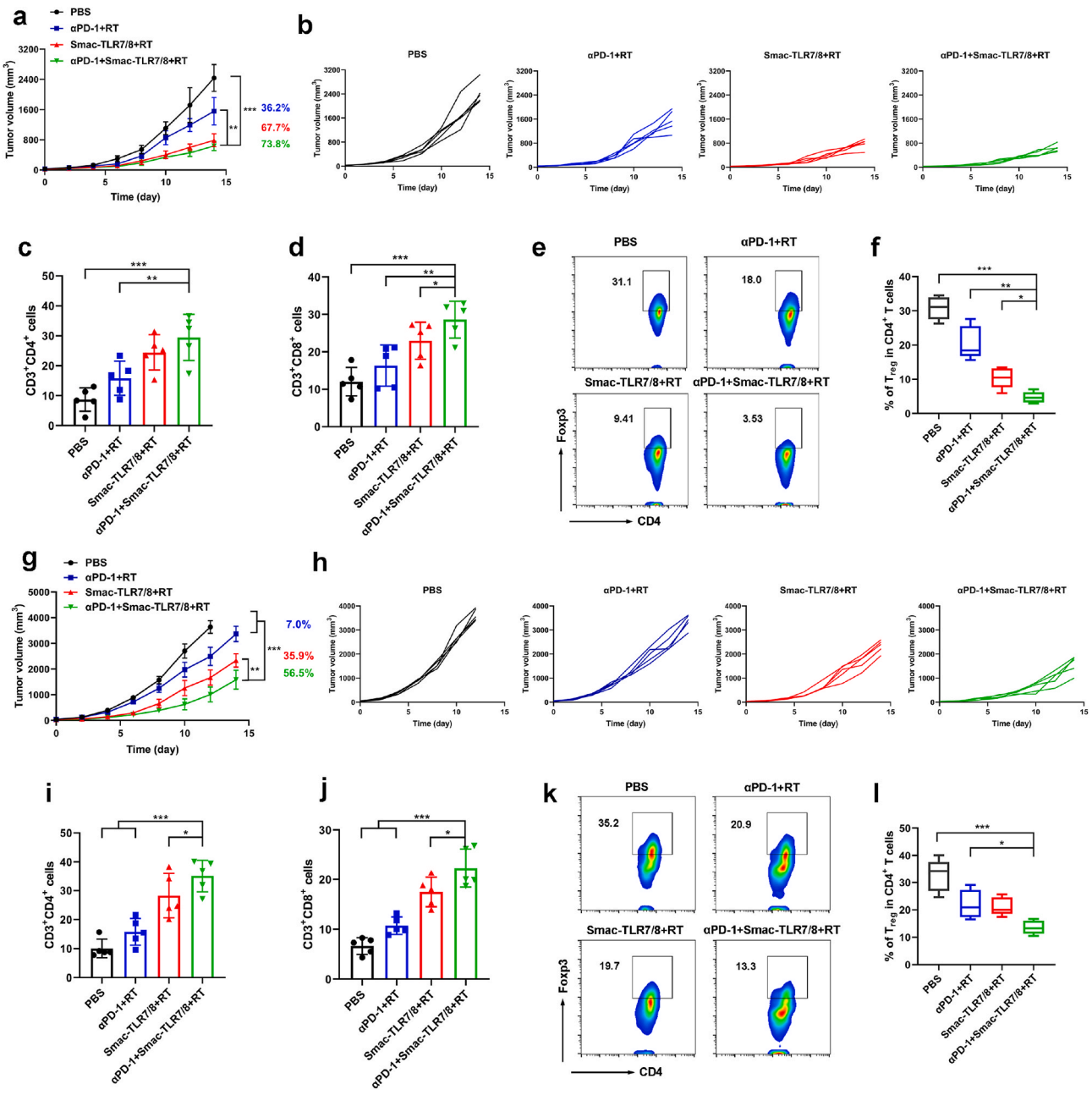

Fig. 5. In vivo tumor treatment of Smac-TLR7/8 hydrogel combined with αPD-1 during radiotherapy. Overall tumor volume curves (a) and individual tumor volume curve (b) of B16 bearing tumor mice (n = 5). The numbers represented for tumor inhibition of different treatment groups. Percentage of $CD3^+CD4^+$ (c) and $CD3^+CD8^+$ T cells (d) (n = 5). **p < 0.01, ***p < 0.001. (e) Flow cytometry analysis of regulatory ($CD4^+Foxp3$) T cells. (f) Percentage of regulatory ($CD4^+Foxp3$) T cells (n = 5). *p < 0.05, **p < 0.01, ***p < 0.001. Overall tumor volume curves (g) and individual tumor volume curve (h) of 4T1 bearing tumor mice (n = 5). The numbers represented for tumor inhibition of different treatment groups. Percentage of $CD3^+CD4^+$ (i) and $CD3^+CD8^+$ T cells (j) (n = 5). **p < 0.01, ***p < 0.001. (k) Flow cytometry analysis of regulatory ($CD4^+Foxp3$) T cells. (l) Percentage of regulatory ($CD4^+Foxp3$) T cells (n = 5). *p < 0.05, ***p < 0.001.

order to further provide an insight on macrophage - T cell crosstalk in tumor microenvironment, the expressions of granzyme B and perforin were supplemented by immunofluorescence staining. Granzyme B is a serine protease found in the cytoplasmic granules of cytotoxic lymphocytes and natural killer cells. Perforin permits delivery of the cytotoxic granzymes A and B into target cells to induce apoptosis and cause cancer cell death. As shown in Fig. S17, after treated with αPD-1+Smac-TLR7/8+RT, the expressions of both granzyme B and perforin in tumor tissues were higher than that of Smac-TLR7/8+RT and αPD-1+RT treatment, suggesting the enhanced antitumor activity of $CD8^+$ T cells.

Next, we evaluated its antitumor efficacy on a 4T1 tumor mice model with low immune activity. As shown in Fig. 5g and h, the antitumor effect was similar to the inhibition tendency on B16 tumor depicted above, but displayed a correspondingly lower tumor inhibition rate. Only 7% of tumor inhibition rate of αPD-1+RT further confirmed that 4T1 tumor mice model is poor in immune activity. But the superior antitumor effect was still achieved by the Smac-TLR7/8+RT (Fig. 5i–j, and Figs. S18–S20), which exhibited correspondingly higher tumor inhibition rate (35.9%) than that of αPD-1+RT treatment, owing to the elimination of tumor radioresistance by significant downregulating expression of Tregs (Fig. 5k and l). It is worth noting that the tumor inhibition rate was further increased to 56.5% after the treatment of αPD-1+Smac-TLR7/8+RT, indicating that TAMs repolarization played

an important role in overcoming tumor radioresistance by rebuilding ITM in the tumor bearing mice model with lower immune activity.

In order to highlight the advantages and clinical perspective of the synergistic effect, the survival rate after different treatments were evaluated in both B16 and 4T1 tumor mice models. As shown in Fig. S21, compared with other groups, treatment with αPD-1+Smac-TLR7/8+RT showed the highest survival rate of B16-bearing mice (80%) and 4T1-bearing mice (90%), which were attributed to the slow growth of tumors. Additionally, there was no obvious change in the body weight during the treatments (Fig. S22). And HE staining of main organs shown in Figs. S23 and S24 also showed no severe side effects after 14 days treatment in vivo, guaranteeing the biosafety.

Recent works highlighted the importance of reprogramming the TAMs into M1 type in improving immunotherapy response and anticancer efficacy [24]. Herein, we are focusing on TAMs repolarization to overcome tumor resistance by rebuilding ITM. We firstly prepared a novel nanofiber hydrogel with conjugation with TLR7/8 agonist and a pro-apoptosis peptide (Smac). The in vitro results in Fig. 2 demonstrated that the Smac-TLR7/8 hydrogel with radiation was able to repolarize the M2 TAMs to M1 type, and further enhanced the antitumor functions of macrophages, including secreting tumor necrosis factor, direct phagocytosis of cancer cells and increasing the radiosensitivity of cancer cells (Fig. 3). In addition, introduction of a pro-apoptosis peptide into the hydrogel further enhanced the radiosensitive effect of Smac-TLR7/8 hydrogel during RT. Therefore, in combination with RT, the TAMs repolarization mediated by Smac-TLR7/8 hydrogel could achieve high antitumor efficiency through eliciting effective antitumor immune response by increasing TILs and downregulating Treg cells in vivo. Considering that radiotherapy and immune checkpoint therapy are current clinical and pre-clinical hot issues. However, the combined treatment effect is limited by the immunosuppressive microenvironment and radiotherapy tolerance, which are closely related [46,47]. Therefore, we further combined immune checkpoint blockade with Smac-TLR7/8 hydrogel+RT treatment to evaluate the antitumor efficiency within tumor mice models with different immune activity. Results in Fig. 5 indicated that the combination therapy was capable of reducing tumor Treg cells, improving immune response, and overcoming radiotherapy resistance, thereby significantly inhibiting tumor growth, which suggested the importance of TAMs reprogramming in clinical tumor therapy. Certainly, although the polarization effect and mechanism of TLR agonists on macrophages are well documented, the effect and mechanism of radiation on the polarization of macrophages is still controversial, including irradiation dose, irradiation method (locally or whole body), and radiation type (α, β, γ radiation). Therefore, in order to promote the clinical application in some complicated tumors (such as pan-cancers) of Smac-TLR7/8 hydrogel+RT treatment, the parameters of combination therapy including radiation type, irradiation dose, and dose of agonists, and even its mechanism need to be further optimized and studied in detail. Furthermore, DNA repair after RT also plays an important role in tumor radioresistance, such as homologous recombination (HR) pathway and non-homologous end joining (NHEJ) [48]. We demonstrated that macrophages polarization could enhance the radiosensitivity through aggravating DNA breakage (Fig. 3g and h). Thus, the molecular biological mechanism (genetic level) of macrophage polarization in overcoming tumor radioresistance may be involved with inhibition of DNA repair during radiotherapy [48,49].

4. Conclusion

In this study, an effective strategy of overcoming radioresistance by rebuilding ITM through regulating macrophage polarization was developed based on the TLR7/8-conjugated radiosensitive peptide hydrogel (Smac-TLR7/8 hydrogel). The Smac-TLR7/8 hydrogel successfully regulated macrophage polarization from a pro-tumor (M2-type) to an antitumor (M1-type) state by activating NF-κB pathway, to further enhance the cytotoxicity, phagocytosis, and DNA damage during RT in vitro. Importantly, this strategy of TAMs repolarization achieved ITM reconstruction by upregulating M1 type TAMs and downregulating M2 type TAMs, increasing TILs, and especially decreasing expression of Treg cells in vivo antitumor treatment, thus showing positively effective tumor inhibition rate and overcoming radioresistance. Meanwhile, the combination of the immune checkpoint inhibitor (αPD-1) and Smac-TLR7/8 hydrogel with radiation, αPD-1 further increased TILs and decreased Treg cells, especially in the tumor-bearing mice model with lower immune activity. Therefore, the combination between nanodrug and immunotherapy may be an ideal therapeutic chance for enhancing ITM construction and overcoming radioresistance.

CRediT authorship contribution statement

Yumin Zhang: Conceptualization, Investigation, Writing – original draft. **Zujian Feng:** Conceptualization, Investigation, Writing – original draft. **Jinjian Liu:** Investigation, Data curation. **Hui Li:** Investigation, Visualization. **Qi Su:** Investigation, Visualization. **Jiamin Zhang:** Software, Writing – review & editing. **Pingsheng Huang:** Software, Writing – review & editing. **Weiwei Wang:** Supervision, Writing – review & editing, Funding acquisition. **Jianfeng Liu:** Supervision, Writing – review & editing, Funding acquisition.

Declaration of competing interest

The authors declare that they have no known competing financial interests or personal relationships that could have appeared to influence the work reported in this paper.

Acknowledgements

This study was financially supported by the National Natural Science Foundation of China (No. 81971731, 82001963, 82172082), PUMC Youth Fund and the Fundamental Research Funds for the Central Universities (No.3332020058), the Non-profit Central Research Institute Fund of Chinese Academy of Medical Sciences (2018PT35031), the Natural Science Fund for Distinguished Young Scholars of Tianjin (18JCJQJC47300) and the CAMS Innovation Fund for Medical Sciences (2021-I2M−042).

Appendix A. Supplementary data

Supplementary data to this article can be found online at https://doi.org/10.1016/j.bioactmat.2021.12.033.

References

[1] C. Allen, S. Her, D.A. Jaffray, Radiotherapy for cancer: present and future, Adv. Drug Deliv. Rev. 109 (2017) 1–2.
[2] J.S. Vaidya, M. Bulsara, F. Wenz, J.S. Tobias, D. Joseph, M. Baum, Targeted radiotherapy for early breast cancer, Lancet 391 (10115) (2018) 26–27.
[3] A.C. Wilkins, E.C. Patin, K.J. Harrington, A.A. Melcher, The immunological consequences of radiation-induced DNA damage, J. Pathol. 247 (5) (2019) 606–614.
[4] J. Marill, N. Mohamed Anesary, S. Paris, DNA damage enhancement by radiotherapy-activated hafnium oxide nanoparticles improves cGAS-STING pathway activation in human colorectal cancer cells, Radiother. Oncol. 141 (2019) 262–266.
[5] M.Y. Ali, C.R. Oliva, A.S.M. Noman, B.G. Allen, P.C. Goswami, Y. Zakharia, V. Monga, D.R. Spitz, J.M. Buatti, C.E. Griguer, Radioresistance in glioblastoma and the development of radiosensitizers, Cancers 12 (9) (2020).
[6] Y. Woo, H.J. Lee, Y.M. Jung, Y.J. Jung, mTOR-mediated antioxidant activation in solid tumor radioresistance, J. Oncol. 2019 (2019), 5956867.
[7] H.E. Barker, J.T. Paget, A.A. Khan, K.J. Harrington, The tumour microenvironment after radiotherapy: mechanisms of resistance and recurrence, Nat. Rev. Cancer 15 (7) (2015) 409–425.
[8] F-l Qi, M-f Wang, B-z Li, Z-f Lu, G-j Nie, S-p Li, Reversal of the immunosuppressive tumor microenvironment by nanoparticle-based activation of immune-associated cells, Acta Pharmacol. Sin. 41 (7) (2020) 895–901.
[9] S.F. Ngiow, A. Young, Re-education of the tumor microenvironment with targeted therapies and immunotherapies, Front. Immunol. 11 (2020) 1633.

[10] K. Shimizu, T. Iyoda, M. Okada, S. Yamasaki, S.I. Fujii, Immune suppression and reversal of the suppressive tumor microenvironment, II (Int. Immunol.) 30 (10) (2018) 445–454.
[11] S.H. van der Burg, R. Arens, F. Ossendorp, T. van Hall, C.J. Melief, Vaccines for established cancer: overcoming the challenges posed by immune evasion, Nat. Rev. Cancer 16 (4) (2016) 219–233.
[12] H. Song, Q. Su, P. Huang, C. Zhang, W. Wang, Self-assembling, self-adjuvanting and fully synthetic peptide nanovaccine for cancer immunotherapy, Smart. Mater. Med 2 (2021) 237–249.
[13] Y. Wang, Z.G. Liu, H. Yuan, W. Deng, J. Li, Y. Huang, B.Y.S. Kim, M.D. Story, W. Jiang, The reciprocity between radiotherapy and cancer immunotherapy, Clin. Cancer Res. 25 (6) (2019) 1709–1717.
[14] G. Genard, S. Lucas, C. Michiels, Reprogramming of tumor-associated macrophages with anticancer therapies: radiotherapy versus chemo- and immunotherapies, Front. Immunol. 8 (2017) 828.
[15] M. Cully, Cancer: Re-educating tumour-associated macrophages with nanoparticles, Nat. Rev. Drug Discov. 17 (7) (2018) 468.
[16] D.G. DeNardo, B. Ruffell, Macrophages as regulators of tumour immunity and immunotherapy, Nat. Rev. Immunol. 19 (6) (2019) 369–382.
[17] E. Persa, A. Balogh, G. Safrany, K. Lumniczky, The effect of ionizing radiation on regulatory T cells in health and disease, Cancer Lett. 368 (2) (2015) 252–261.
[18] A. Oweida, M.K. Hararah, A. Phan, D. Binder, S. Bhatia, S. Lennon, S. Bukkapatnam, B. Van Court, N. Uyanga, L. Darragh, H.M. Kim, D. Raben, A. C. Tan, L. Heasley, E. Clambey, R. Nemenoff, S.D. Karam, Resistance to radiotherapy and PD-L1 blockade is mediated by TIM-3 upregulation and regulatory T-cell infiltration, Clin. Cancer Res. 24 (21) (2018) 5368–5380.
[19] M.M. Leblond, E.A. Peres, C. Helaine, A.N. Gerault, D. Moulin, C. Anfray, D. Divoux, E. Petit, M. Bernaudin, S. Valable, M2 macrophages are more resistant than M1 macrophages following radiation therapy in the context of glioblastoma, Oncotarget 8 (42) (2017) 72597–72612.
[20] J.G. Price, J. Idoyaga, H. Salmon, B. Hogstad, C.L. Bigarella, S. Ghaffari, M. Leboeuf, M. Merad, CDKN1A regulates Langerhans cell survival and promotes Treg cell generation upon exposure to ionizing irradiation, Nat. Immunol. 16 (10) (2015) 1060–1068.
[21] D.S. Kim, H. Dastidar, C. Zhang, F.J. Zemp, K. Lau, M. Ernst, A. Rakic, S. Sikdar, J. Rajwani, V. Naumenko, D.R. Balce, B.W. Ewanchuk, P. Tailor, R.M. Yates, C. Jenne, C. Gafuik, D.J. Mahoney, Smac mimetics and oncolytic viruses synergize in driving anticancer T-cell responses through complementary mechanisms, Nat. Commun. 8 (1) (2017) 344.
[22] J. Liu, Y. Zhang, Q. Li, Z. Feng, P. Huang, W. Wang, J. Liu, Development of injectable thermosensitive polypeptide hydrogel as facile radioisotope and radiosensitizer hotspot for synergistic brachytherapy, Acta Biomater. 114 (2020) 133–145.
[23] S. Fulda, Promises and challenges of smac mimetics as cancer therapeutics, Clin. Cancer Res. 21 (22) (2015) 5030–5036.
[24] C.B. Rodell, S.P. Arlauckas, M.F. Cuccarese, C.S. Garris, R. Li, M.S. Ahmed, R. H. Kohler, M.J. Pittet, R. Weissleder, TLR7/8-agonist-loaded nanoparticles promote the polarization of tumour-associated macrophages to enhance cancer immunotherapy, Nat. Biomed. Eng. 2 (8) (2018) 578–588.
[25] Y. Feng, R. Mu, Z. Wang, P. Xing, J. Zhang, L. Dong, C. Wang, A toll-like receptor agonist mimicking microbial signal to generate tumor-suppressive macrophages, Nat. Commun. 10 (1) (2019) 2272.
[26] B. Ma, Y. Yang, Z. Li, D. Zhao, W. Zhang, Y. Jiang, D. Xue, Modular bioinformatics analysis demonstrates that a Tolllike receptor signaling pathway is involved in the regulation of macrophage polarization, Mol. Med. Rep. 18 (5) (2018) 4313–4320.
[27] K. Taniguchi, M. Karin, NF-kappaB, inflammation, immunity and cancer: coming of age, Nat. Rev. Immunol. 18 (5) (2018) 309–324.
[28] H. Xiao, Y. Guo, B. Li, X. Li, Y. Wang, S. Han, D. Cheng, X. Shuai, M2-Like tumor-associated macrophage-targeted codelivery of STAT6 inhibitor and IKKbeta siRNA induces M2-to-M1 repolarization for cancer immunotherapy with low immune side effects, ACS Cent. Sci. 6 (7) (2020) 1208–1222.
[29] L. Li, M. Zhen, H. Wang, Z. Sun, W. Jia, Z. Zhao, C. Zhou, S. Liu, C. Wang, C. Bai, Functional gadofullerene nanoparticles trigger robust cancer immunotherapy based on rebuilding an immunosuppressive tumor microenvironment, Nano Lett. 20 (6) (2020) 4487–4496.
[30] Z. Feng, Q. Su, C. Zhang, P. Huang, H. Song, A. Dong, D. Kong, W. Wang, Bioinspired nanofibrous glycopeptide hydrogel dressing for accelerating wound healing: a cytokine-free, M2-type macrophage polarization approach, Adv. Funct. Mater. 30 (52) (2020), 2006454.
[31] Q. Wang, M. Xiao, D. Wang, X. Hou, J. Gao, J. Liu, J. Liu, In situ supramolecular self-assembly of Pt(IV) prodrug to conquer cisplatin resistance, Adv. Funct. Mater. 31 (27) (2021), 2101826.
[32] P. Yang, H. Song, Z. Feng, C. Wang, P. Huang, C. Zhang, D. Kong, W. Wang, Synthetic, supramolecular, and self-adjuvanting CD8+ T-cell epitope vaccine increases the therapeutic antitumor immunity, Adv. Ther. (2019), 1900010.
[33] M. Li, P. Liu, G. Gao, J. Deng, Z. Pan, X. Wu, G. Xie, C. Yue, C.H. Cho, Y. Ma, L. Cai, Smac therapeutic Peptide nanoparticles inducing apoptosis of cancer cells for combination chemotherapy with Doxorubicin, ACS Appl. Mater. Interfaces 7 (15) (2015) 8005–8012.
[34] K. Ni, T. Luo, A. Culbert, M. Kaufmann, X. Jiang, W. Lin, Nanoscale metal-organic framework Co-delivers TLR-7 agonists and anti-CD47 antibodies to modulate macrophages and orchestrate cancer immunotherapy, J. Am. Chem. Soc. 142 (29) (2020) 12579–12584.
[35] Q. Wang, N. Jiang, B. Fu, F. Huang, J. Liu, Self-assembling peptide-based nanodrug delivery systems, Biomater. Sci. 7 (12) (2019) 4888–4911.
[36] C. Ren, Z. Wang, Q. Wang, C. Yang, J. Liu, Self-assembled peptide-based nanoprobes for disease theranostics and disease-related molecular imaging, Small Methods 4 (4) (2020), 1900403.
[37] Y. Zhou, X. Chen, Z. Cao, J. Li, H. Long, Y. Wu, Z. Zhang, Y. Sun, R848 is involved in the antibacterial immune response of golden pompano (Trachinotus ovatus) through TLR7/8-MyD88-NF-κb-signaling pathway, Front. Immunol. 11 (3499) (2021), 617522.
[38] A. Mantovani, F. Marchesi, A. Malesci, L. Laghi, P. Allavena, Tumour-associated macrophages as treatment targets in oncology, Nat. Rev. Clin. Oncol. 14 (7) (2017) 399–416.
[39] L. Yang, J. Sun, Q. Liu, R. Zhu, Q. Yang, J. Hua, L. Zheng, K. Li, S. Wang, A. Li, Synergetic functional nanocomposites enhance immunotherapy in solid tumors by remodeling the immunoenvironment, Adv. Sci. 6 (8) (2019), 1802012.
[40] X. Xu, X. Gong, Y. Wang, J. Li, H. Wang, J. Wang, X. Sha, Y. Li, Z. Zhang, Reprogramming tumor associated macrophages toward M1 phenotypes with nanomedicine for anticancer immunotherapy, Adv. Ther. 3 (5) (2020), 1900181.
[41] L. Rao, S.-K. Zhao, C. Wen, R. Tian, L. Lin, B. Cai, Y. Sun, F. Kang, Z. Yang, L. He, J. Mu, Q.-F. Meng, G. Yao, N. Xie, X. Chen, Activating macrophage-mediated cancer immunotherapy by genetically edited nanoparticles, Adv. Mater. 32 (47) (2020), 2004853.
[42] Y.R. Zhang, J.Q. Luo, J.X. Li, Q.Y. Huang, X.X. Shi, Y.C. Huang, K.W. Leong, W. L. He, J.Z. Du, Biofunctional Janus particles promote phagocytosis of tumor cells by macrophages, Chem. Sci. 11 (20) (2020) 5323–5327.
[43] X. Chen, E. Fu, H. Lou, X. Mao, B. Yan, F. Tong, J. Sun, L. Wei, IL-6 induced M1 type macrophage polarization increases radiosensitivity in HPV positive head and neck cancer, Cancer Lett. 456 (2019) 69–79.
[44] L. Portella, S. Scala, Ionizing radiation effects on the tumor microenvironment, Semin. Oncol. 46 (3) (2019) 254–260.
[45] Q. Zhu, X. Wu, Y. Wu, X. Wang, Interaction between Treg cells and tumor-associated macrophages in the tumor microenvironment of epithelial ovarian cancer, Oncol. Rep. 36 (6) (2016) 3472–3478.
[46] A. Oweida, M.K. Hararah, A. Phan, D. Binder, S. Bhatia, S. Lennon, S. Bukkapatnam, B. Van Court, N. Uyanga, L. Darragh, H.M. Kim, D. Raben, A. C. Tan, L. Heasley, E. Clambey, R. Nemenoff, S.D. Karam, Resistance to radiotherapy and PD-L1 blockade is mediated by TIM-3 upregulation and regulatory T-cell infiltration, Clin. Cancer Res. 24 (21) (2018) 5368–5380.
[47] Y. Wang, Z.-G. Liu, H. Yuan, W. Deng, J. Li, Y. Huang, B.Y.S. Kim, M.D. Story, W. Jiang, The reciprocity between radiotherapy and cancer immunotherapy, Clin. Cancer Res. 25 (6) (2019) 1709–1717.
[48] E. Kocakavuk, K.J. Anderson, F.S. Varn, K.C. Johnson, S.B. Amin, E.P. Sulman, M. P. Lolkema, F.P. Barthel, R.G.W. Verhaak, Radiotherapy is associated with a deletion signature that contributes to poor outcomes in patients with cancer, Nat. Genet. 53 (7) (2021) 1088–1096.
[49] W. Zhou, Y. Yao, A.J. Scott, K. Wilder-Romans, J.J. Dresser, C.K. Werner, H. Sun, D. Pratt, P. Sajjakulnukit, S.G. Zhao, M. Davis, B.S. Nelson, C.J. Halbrook, L. Zhang, F. Gatto, Y. Umemura, A.K. Walker, M. Kachman, J.N. Sarkaria, J. Xiong, M. A. Morgan, A. Rehemtualla, M.G. Castro, P. Lowenstein, S. Chandrasekaran, T. S. Lawrence, C.A. Lyssiotis, D.R. Wahl, Purine metabolism regulates DNA repair and therapy resistance in glioblastoma, Nat. Commun. 11 (1) (2020) 3811.